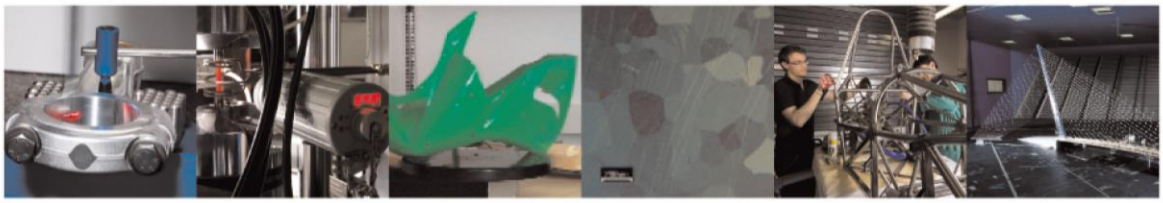

Design of Deformable Tools for Sheet Metal Forming

Iorio, Lorenzo; Pagani, Luca; Strano, Matteo; Monno, Michele

This is a post-peer-review, pre-copyedit version of an article published in JOURNAL OF MANUFACTURING SCIENCE AND ENGINEERING, 140/4, on February 5, 2018. The final authenticated version is available online at: http://dx.doi.org/10.1115/1.4034006

https://asmedigitalcollection.asme.org/manufacturingscience/article/doi/10.1115/1.4034006/472551/Design-of-Deformable-Tools-for-Sheet-Metal-Forming

DIPARTIMENTO DI MECCANICA ■ POLITECNICO DI MILANO
via G. La Masa, 1 ■ 20156 Milano ■ EMAIL (PEC): pecmecc@cert.polimi.it
http://www.mecc.polimi.it
Rev. 0

DESIGN OF DEFORMABLE TOOLS FOR SHEET METAL FORMING

Lorenzo Iorio
MUSP Lab.
Piacenza, Italy
lorenzo.iorio@musp.it

Luca Pagani
University of Huddersfield
Huddersfield, United Kingdom
l.pagani@hud.ac.uk

Matteo Strano and Michele Monno
Politecnico di Milano, Dipartimento di Meccanica
Milan, Italy
matteo.strano@polimi.it, michele.monno@polimi.it

ABSTRACT

Traditionally, industrial sheet metal forming technologies use rigid metallic tools to plastically deform the blanks. In order to reduce the tooling costs, rubber or flexible tools can be used together with one rigid (metallic) die or punch, in order to enforce a predictable and repeatable geometry of the stamped parts. If the complete tooling setup is built with deformable tools, the final part quality and geometry are hardly predictable and only a prototypal production is generally possible. The aim of this paper is to present the development of an automatic tool design procedure, based on the explicit FEM simulation of a stamping process, coupled to a geometrical tool compensation algorithm. The FEM simulation model has been first validated by comparing the experiments done at different levels of the process parameters. After the experimental validation of the FEM model, a compensation algorithm has been implemented for reducing the error between the simulated component and the designed one. The tooling setup is made of machined thermoset polyurethane punch, die and blankholder, for the deep drawing of an aluminum part. With respect to conventional steel dies, the plastic tools used in the test case are significantly more economic. The proposed procedure is iterative. It allows, already after the first iteration, to reduce the geometrical deviation between the actual stamped part and the designed geometry. This methodology represents one step towards the transformation of the investigated process from a prototyping technique into an industrial process for small and medium batch sizes.

INTRODUCTION

In the conventional deep drawing and stamping processes, a tooling setup made of a die, a punch and a blankholder is traditionally used. Over the years, many different types of flexible sheet forming processes have been developed in the industry, in order to improve the process, and especially in order to compress the tooling production times and costs. Single point and double point incremental forming processes [1] have been invented and are continuously being developed to this purpose. As another cost saving option, one or more of the metal tools are replaced with a rubber membrane. The Guerin process makes use of a movable thick rubber pad pressed against a die [2-3] or punch [4-5]. The Marform process is a variant of the Guerin, using an active blankholder [6]. In flexforming with a fluid cell, a rubber diaphragm is pressurized by a fluid or by a bladder [7]. In deep drawing flexforming, a movable punch is used, too [8]. In multi-point stretch forming [9], stretch forming clamps are used with the sheet bent over a flexible die made by a raster of metallic movable pins. Most of these applications have been developed and are largely used in the aerospace industry, due to their low tooling cost, which is very convenient in the production of small batches.

Normally, these processes involve using a metallic tool (punch or die) and a counter-rubber-die with "general purpose" shape, due to the high deformation capacity of the elastomeric material, e.g. a membrane or a cushion.

In the last few years, the tremendous growth of additive manufacturing technologies is changing completely the way of thinking about functional parts and designing them. At the same time, a reborn attention is being given to rapid tooling technologies [10], which offer cost-efficient and innovative solutions for improving the sheet metal forming processes.

An interesting application can be found in [11] where a Nylon66 membrane and PTFE die are applied in a deep drawing process, in order to avoid the wrinkling effect and increasing the lubrication of the process due to the PTFE material properties.

The rapid tooling method proposed in the present work is to machine polymeric boards which, in a few minutes, can be transformed into a forming tooling setup (punches, dies and blank-holder). One of the previous research works concerning all-polymeric forming tools with experimental and numerical analysis are by Park and Colton of Georgia Tech [12-14] in the mid of years 2000. Sheet metal forming processes performed only with plastics tools are used as prototyping methods, i.e. in prototyping job shops or for artistic uses by jewellers and metalsmiths [15]. Some investigations have been conducted for commercial application in case of automotive sheet metal components made by FDM rapid prototype tools [16]. The rapid tools are used also in Hydroforming automotive applications for producing engine cradles, suspension components, radiator and instrument panel support beams and engine components [17]. The use of flexible tools as a true industrialised technique is limited by two main drawbacks: 1) the final geometry of the formed part is difficult to predict, because of the elastic deflection of the tools; 2) polymeric punches and dies are subject to early wearing and failure mechanisms, if compared to classic metal tools and, therefore, intended for single parts or very small batches. A study has been conducted for increasing the performance of the Rapid Tools made of coated polymers, by reinforcing the surface with a hard coating obtained by indirect spraying. The research work of J. Witulski et al. [18] demonstrates that reinforced Rapid Tools can be applied in small and medium batch productions of high strength materials.

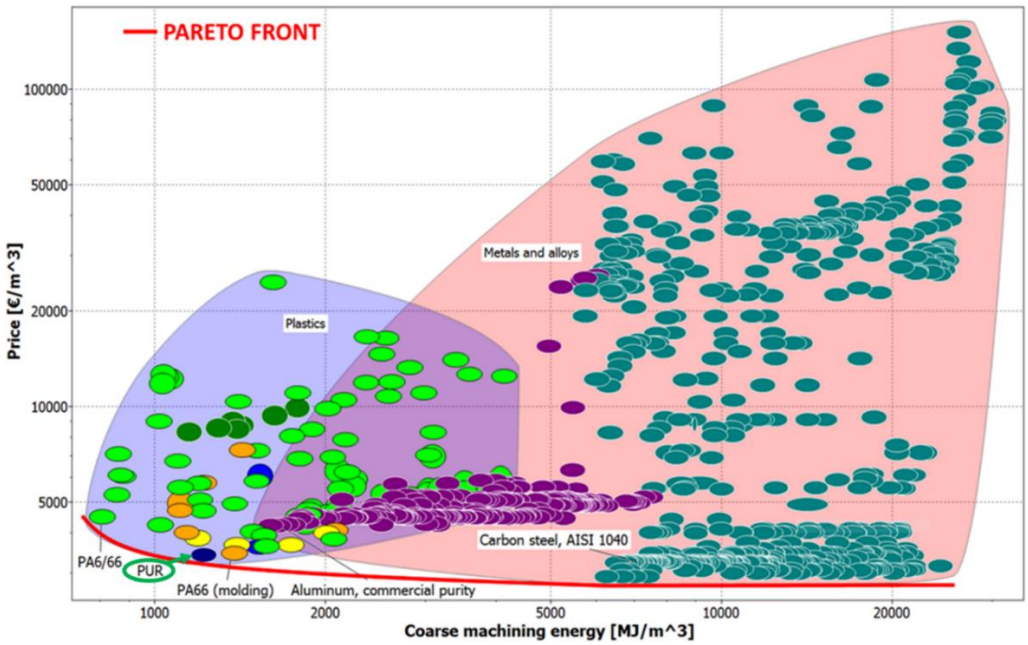

FIG. 1: MATERIALS COMPARISON PRICE VS. COARSE MACHINING ENERGY - DATA COMING FROM CES EDUPACK 2015.

The purpose of the present paper is to face the first issue, i.e. to solve the geometrical predictability problem, by using CAE in combination with a compensation technique. The approach is to predict the actual deformation of the tools and to determine their compensation in case the part falls outside the initial design tolerances.

The main advantage in using rapid polymeric tools is due to their low required machining energy and cost. FIG. 1 shows a comparison between the traditional tool steels and the rapid tool materials. In the graph a Pareto Front is highlighted, in order to identify the set of materials with the lower buying price (€/m³) and lower coarse machining energy (MJ/m³). The figure shows that polyurethane (PUR) is one of the most interesting locations on the Pareto Front. The most expensive material used in this paper (commercial name Necuron 1300) has a comparable cost per unit volume, expressed in €/m^3, to an AISI 1040 steel. However, the material removal rate in machining is more than 4 times faster, with a negligible tool wear.

As stated above, the purpose of the present paper is to develop a die compensation technique, based on FEM simulations, which takes into account the deformability of both the tools and the blank. The scientific literature on numerical die compensation methods is wide. Some of the more recent and relevant works in this field will be now very briefly cited.

The most frequently used methods for die compensation are the displacement adjustment (DA), the surface controlled overbending (SCO) and the Force Descriptor Method (FDM).

The displacement adjustment is probably the most effective method; the tools nodes are displaced in the opposite direction of the blank springback [19]. The deviations calculation is done between the correspondent nodes of the simulated and the designed blank. This means that no remeshing is possible or, alternatively, any new mesh must be remapped with reference to the mesh of the designed part. For this reason, the DA method is frequently used for simple 2D forming cases [20], where a small number of nodes must be mapped or remeshing is not even required.

The surface controlled overbending algorithm performs the calculation directly on the tools CAD but, again, the calculation complexity makes the method inaccurate on a complex surface with high degree [21].

The Force Descriptor Method proposed by Karafillis and Boyce [22] is an iterative method based on the evaluation of the internal forces of the component, but the algorithm suffers from lack of convergence, especially in symmetric cases or limit values of springback.

The purpose of the paper is to present a compensation algorithm and FEM model, which will allows to evaluate the effective deformation of the tools and to determine their compensation in case the part falls outside the initial design tolerances. The proposed algorithm is inspired by the DA method, but improves the distance calculation by evaluating the normal distance from the tools node to the interpolated blank surfaces. Unlike the standard DA, there is no need to keep track of predetermined couples of nodes. The calculation of the normal distance will solve the main disadvantage of the DA algorithm, allowing the applicability of the method also for 3D complex components. The present work is an evolution of the preliminary results already presented by the authors in [23]. The same test case has been used, but the FEM model has been improved and better validated; besides, the compensation algorithm has been significantly modified and the results are different and better.

In the following Sections we will describe the experimental test case and the FEM model. Then, we will present the results of the FEM model validation. After the validation, the development of the compensation algorithm will be described, in terms of mathematical formulation and algorithmic solutions. Finally, the compensation results will be presented.

DESCRIPTION OF THE EXPERIMENTAL TEST CASE

The test case (FIG. 2) is a stamped component, where we can identify one symmetry plane and some geometrical features, which are predictably hard to be obtained in a stamping process with flexible tools. The constant radii (R10 in Fig. 2) are very small, i.e. difficult to be obtained in this kind of processes, because the deformable tools usually tend to slightly deform by compression in corner regions.

The material chosen for the test case is Al1050, annealed, with 2 mm wall thickness. The reference geometry of the part, which will be called "designed geometry", is the starting point for determining the geometry of the deformable tools. An initial guess geometry of the deformable tools is built as an offset of the surfaces of the test case part; the iterative compensation algorithm will suggest a modification of this initial geometry.

The deformable tooling setup (FIG. 3) is composed by the die, the blankholder (green tools) and the punch (orange tool). The polyurethane materials chosen for testing the deformable tools are: Necuron 1050 for the die and blankholder; Necuron 1300 for the punch. The material properties are discussed in the following Section. The estimated cost of the punch is about € 800 (including machining costs). The same punch, made by an AISI 1040 steel would cost about € 4600.

FIG. 3 shows the direction of the stamping process. The steps of the stamping process studied in this article can be summarized as follows:

1. *Holding*: the blank is placed on the blankholder and then the die moves downward for holding it;
2. *Stamping*: the die pushes down the blank and the blankholder on the punch; in this step the blankholder applies a force towards the stamping direction, for controlling the draw-in of the blank during the stamping operation in order to prevent the onset of wrinkling.
3. *Springback*: the tools are released and the blank tends to return to the initial state due to the residual stresses generated by the stamping operation.

The test case described here has been stamped on a hydraulic press (Fig. 4a), which allows to apply up to 1500 kN on the die side and up to 46 kN on the blankholder side. While the die moves downward with a controlled displacement, the punch is fixed and the blankholder opposes a reaction force BHF, with a peak value BHF_{max}. An experimental plan has been designed with 5 variable levels of the blankholder force. Each level has been replicated twice (TABLE 1). The die velocity, the reaction force on the die and the blankholder force have been measured with a sampling frequency of 100 Hz. In Fig. 5, the BHF profiles for experiments no. 3 and 10 (minimum level of BHF) and for experiments 4 and 9 (maximum BFH) are shown. The graphs indicate that there is a very good reproducibility of the tests, at least with respect to forces.

The plan has been designed in order to determine which level of maximum blankholder force could determine failure of the parts (by either wrinkling or fracture) OR failure of the tools (by fracture or plasticization). The plan was also meant to produce different degrees of errors of the stamped vs. the designed part.

TABLE 1: EXPERIMENTAL PLAN

Experiment no.	Maximum BHF (kN)
1 and 6	38
2 and 8	40
3 and 10	22
4 and 9	44.5
5 and 7	30

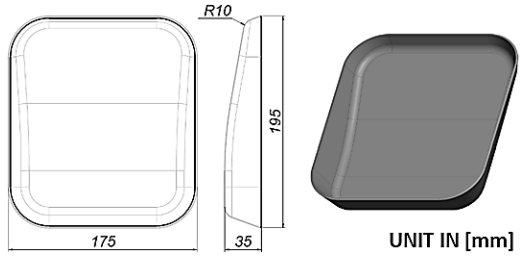

FIG. 2: GEOMETRY OF THE TEST CASE USED FOR DEVELOPING THE OPTIMIZATION ALGORITHM.

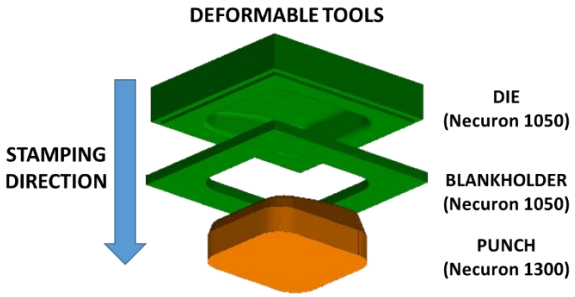

FIG. 3: FLEXIBLE TOOLING SETUP.

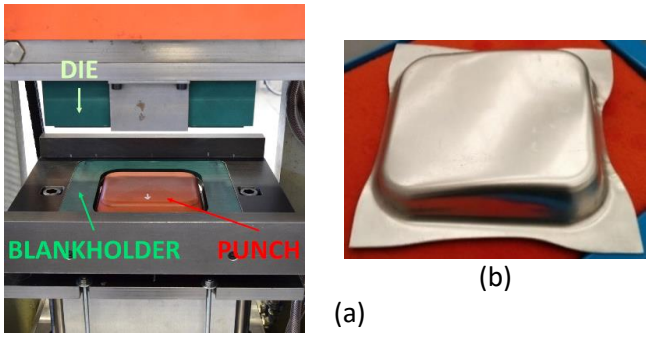

FIG. 4: (a) STAMPING TOOLS MOUNTED ON THE PRESS, PUNCH AND BLANKHOLDER ARE VISIBLE; (b) THE STAMPED COMPONENT MADE WITH THE INITIAL GEOMETRY OF THE TOOLS.

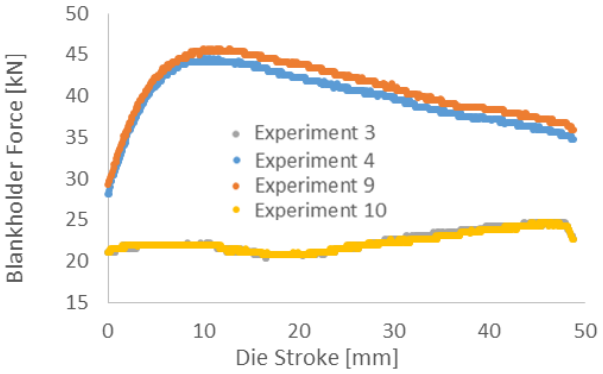

FIG. 5: FORCE PROFILES VS. DIE STROKE.

The experimental results showed that no macroscopic wrinkling occurred at any level of BHF_{max}.
The parts at experiments no. 4-9 failed by fracture, hence the safe limit to fracture for BHF_{max} was assessed at 40 kN. All stamped parts have been measured with a Zeiss Prismo 5 VAST MPS HTG Coordinate Measuring Machine (CMM), obtaining their profile at the symmetry plane. The largest geometrical errors (deviations from the designed geometry) were obtained with a maximum BHF_{max} 22 kN (experiments 3-10). On the other hand, the smallest values of stress on the plastic tools is obviously expected at the minimum possible values of blankholding constraints. Plastic tools that are less stressed during the stamping process will have a longer expected life and will eventually be more cost efficient. In conclusion, the experiments have shown that, with respect to cost efficiency, the best choice of BHF_{max} is located at the minimum value of the range (22 kN). This condition unfortunately induces large geometrical errors. An effective tool shape compensation approach must be implemented, in order to reduce the geometrical errors within tolerance, while still keeping the BHF_{max} value at a low level.

FEM MODEL DESCRIPTION

The FEM model has been implemented with the commercial code PAM-STAMP 2G V2012.2, which allows to define the geometry of the blank directly in the graphical unit interface in a parametric way. For an accurate simulation of the blank deformation during the stamping process, it is necessary to evaluate also the deformation of the tools.

For this reason, the mesh of the polyurethane tools is composed by four-node tetrahedral solid elements. The solid mesh of the plastic tools is created with VisualMesh 11 by using an automatic meshing tool, with proximity and curvature controls. The surface curvature is used to determine the element density (finer mesh is generated in areas of high surface curvature). The number of elements and the number of nodes for each tool is shown in Table 2. A good discretization is important for the accuracy of the FEM simulation, but it is also very important for the application of the compensation algorithm.

The dimensions of the rectangular blank are 125x270 mm and the surface area of each initial element is 345 mm^2 with a total number of 98 initial elements. Every refinement step splits one quadrangular element into four smaller quadrangular shells, by an automatic refinement algorithm. Each element can be split up to 5 times.

TABLE 2: NUMBER OF ELEMENTS AND NODES USED FOR MESHING THE TOOLS.

Tool	N. elements	N. nodes
Die	177083	34568
Blankholder	12260	3524
Punch	194665	36647

TABLE 3: MATERIAL PROPERTIES OF THE POLYURETHANE TOOLS AND ALUMINUM BLANK.

Material	Young Modulus *MPa*	Linear elastic limit *MPa*	Yield Stress *MPa*	Poisson coeff.	Density *g/cm³*
Al1050	72000		33	0.335	2.73
Necuron 1300 (punch)	2317	35	68	0.340	1.15
Necuron 1050 (die)	2922	57	81	0.340	1.20

The tensile test data of the blank have been retrieved in the "CES EduPack" material database, since the Al 1050 is a very common material. Tensile data of the tool materials can be found in the literature too [24]. Compression tests have been performed also on cylindrical samples, which show that the material has a similar compressive elastic modulus. The FEM software used for this research activity calculates the effective stress in a symmetrical way with respect to mean tensile and compressive states of stress. In other words, a unique Young's modulus for tension and compression can be defined. The best obtained values for the elastic modulus and the Poisson coefficient are given in values in Table 3. The blank material is modeled as elastic-plastic. The coefficients of the Krupkowsky's strain hardening law used in the simulations are:

$$\sigma = K \cdot (\varepsilon_0 + \varepsilon_p)^n \qquad (1)$$

with K= 126.7 MPa, n=0.175, ε_0=0.0005.

The simulation starts at the end of the holding stage in which the blank is held between the die and the blankholder (FIG. 6). Then the die moves down with a constant velocity and the blankholder applies the experimentally measured BHF, in order to control the draw-in of the blank.

The contact algorithm between the objects is automatically defined by the software taking into account a Coulomb friction coefficient of 0.25 [11], in order to better simulate the interaction between polyurethane and aluminum materials condition.
As shown in Fig.3a, the plastic tools are enclosed within metal plates which act as connecting elements to the press and as casings for the tools. In order to correctly simulate the effect of

these plates on the deformable tools shown in Fig. 3, proper boundary conditions have been applied only on specific nodes.

For the die, a given velocity is applied on the upper and on some lateral nodes; the force for the blankholder is applied on the lower surface, in order to simulate a uniform distribution of the pressure; finally, a fixed displacement is applied on the lower and some lateral nodes of the punch (Fig. 7a). The springback simulation is run by the FEM software with the "Advanced Implicit" algorithm, by removing three degrees of freedom at two nodal locations on the stamped component, due to the symmetry (Fig. 7b).

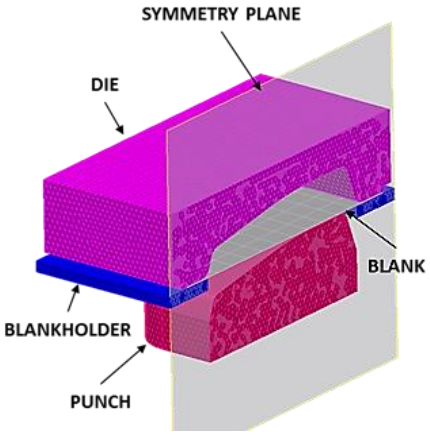

FIG. 6: SCHEME OF THE SIMULATION SETUP AT THE BEGINNING OF THE SIMULATION.

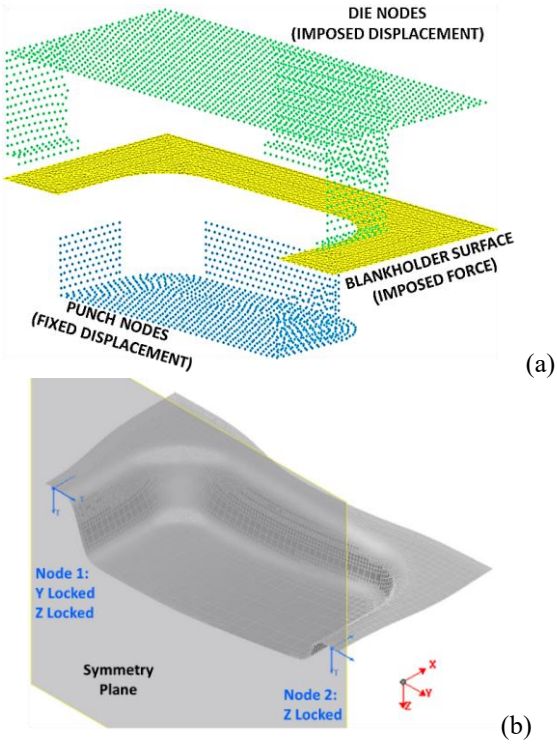

FIG. 7: SCHEMES OF THE NODES AND ELEMENTS WITH BOUNDARY CONDITIONS APPLIED.

VALIDATION RESULTS

In this section, we present the results of the validation of the FEM model, using the experimental values of the stamping process with deformable tools.

As a first way for validating the accuracy of the simulations, the experiment no. 4 is very useful, where the maximum force is applied on the blankholder. In the real tests, fracture occurred at this high level of draw-in restraint. Fortunately, the experiment and the simulation show the same location of the blank fracture localized at the deepest corners of the component (FIG. 8 and Fig. 9). No other simulation nor experimental case had occurrence of fracture.

In order to further validate the results, all stamped components have been measured with the Zeiss CMM in order to measure the profiles along the symmetry plane, to be compared with the FEM simulation. For brevity, only the numerical error on the profiles of experiment no. 3 and 10 are presented in FIG. 10.

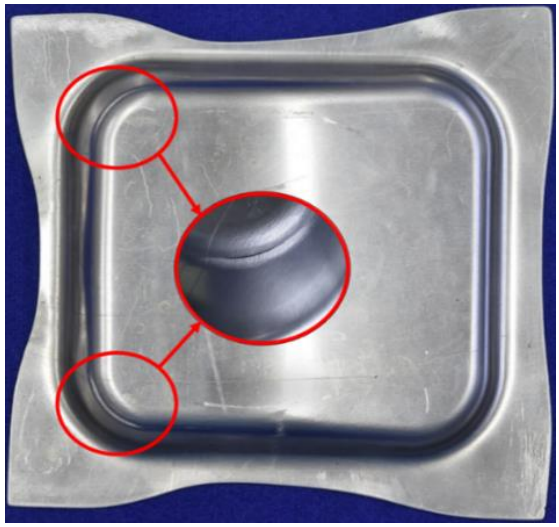

FIG. 8: FRACTURE LOCALIZATION - EXPERIMENT 4

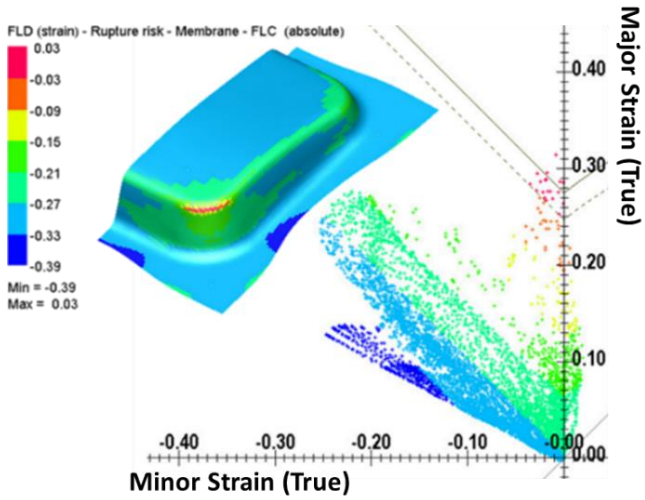

FIG. 9: FLD OF THE EXPERIMENT 4 SIMULATION.

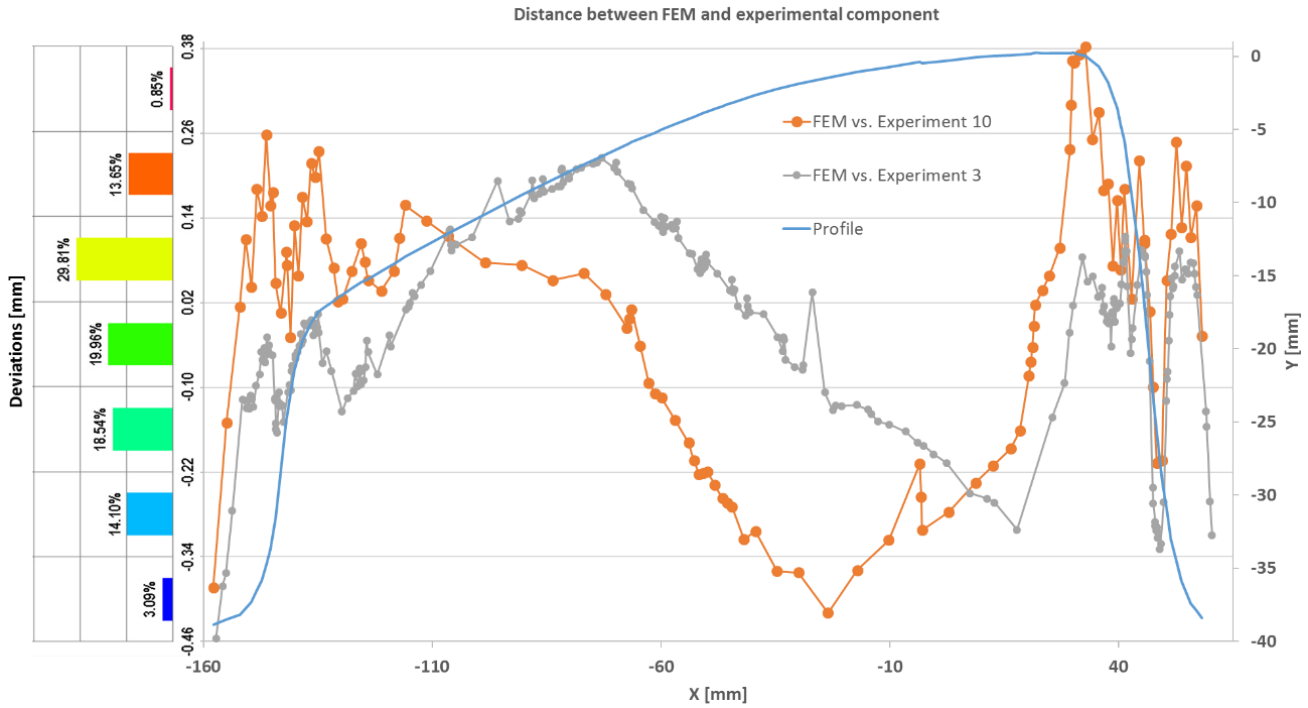

FIG. 10: ERRORS BETWEEN FEM AND EXPERIMENTAL PROFILE FOR EXPERIMENTS 3 AND 10.

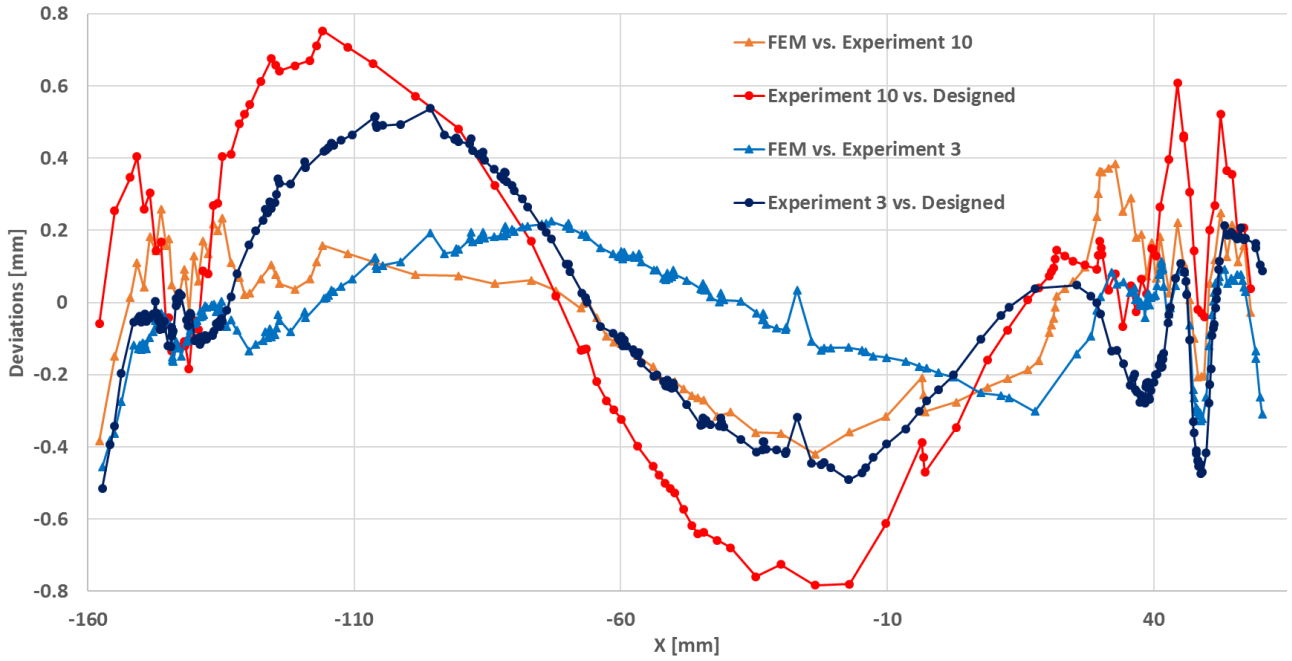

FIG. 11: EXPERIMENTAL VS. FEM ERRORS; EXPERIMENTAL VS. DESIGNED PROFILE DEVIATIONS.

The error between the experimental and numerical profiles are included in the range [-0.46; +0.25] for part 3 and [-0.40; +0.38] for part 10. 81.96 % of the deviation values are included within the interval of [-0.25; +0.25]; the mean of the deviations is -0.01 mm. In absolute terms, smaller error values can be observed close to the locations of the 2 FEM mesh nodes which have been locked in the simulation of springback (see Fig. 7b).

As stated in the previous Section, experiments no. 3-10 form the most interesting test case, because of the low level of stresses on the tools and the corresponding large geometrical deviations

between the stamped and the designed geometries. FIG. 11 shows the deviations between the experimental component and the designed one. In FIG. 11, the range of the error between FEM and experiments (curves with triangles) is smaller than the deviations measured between the experimental and designed profile (curves with circles). In other words, the simulations seem to be accurate enough to allow for an improvement (through die shape compensation) of the stamped geometry.

This test case will also be used when demonstrating the application of the compensation algorithm.

The validation of the FLD map previously shown in Fig. 9 has been done by comparing the strain measured experimentally and the simulated ones. The experimental engineering major and minor strain have been measured with AutoGrid® 3D measuring system made by ViALUX. The AutoGrid® 3D measuring system allows to evaluate the engineering strain on a stamped component previously meshed with a grid pattern. The 3D measuring system evaluates the deformation of the grid pattern on the stamped component and calculates the correspondent deformation in term of engineering strain maps. The comparison between the FEM and AutoGrid® strain maps are shown in Fig. 12. The measured and simulated maps for the major strain compare very well, the two ranges are almost completely overlapped and the color maps are also very similar. As the only clear difference, the AutoGrid® measurements exhibit some localized spots of small negative values (pictured in dark blue), which are probably due to a small measurement error. As for the minor strain maps, they are also very similar, although the FEM is not able to catch some small wrinkling at the flange, where the minimum negative values (pictured in dark blue) have been optically measured.

In conclusion, the good results obtained from the comparisons of profiles and the fracture localization allow to consider the FEM model sufficiently accurate to model the stamping process with polyurethane tools.

COMPENSATION ALGORITHM

The main response variables in a stamping process with deformable tools are the deviations between the geometry of the real *stamped* component and the *designed* one.

In simulations, the deviations will be calculated between the *simulated* and the *designed* parts. These deviations are due mostly to the deformations of the plastic tools during the process and partly to unpredicted springback after the stamping process.

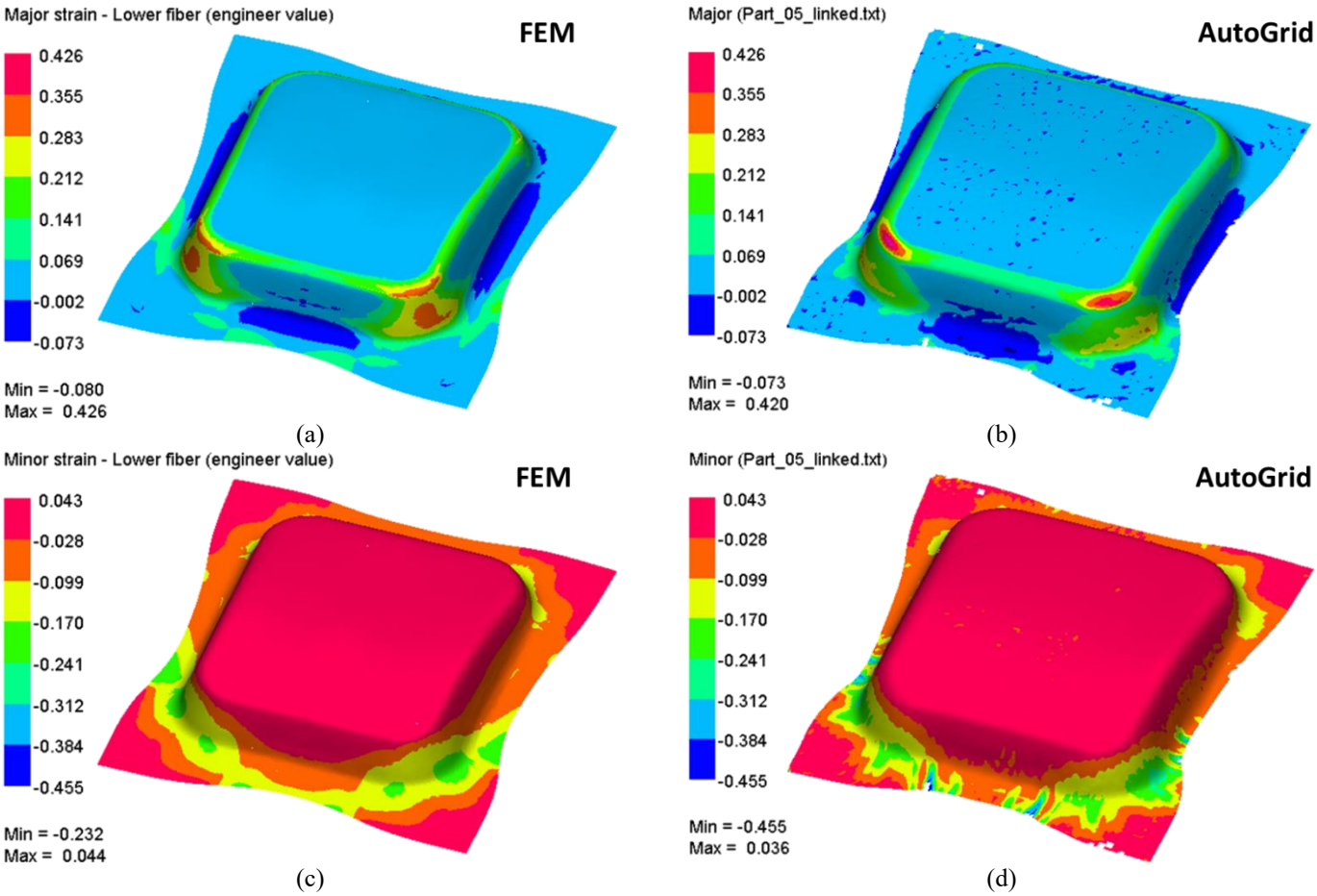

FIG. 12: COMPARISON BETWEEN SIMULATED (A) AND MESURED (B) ENGINEERING MAJOR STRAIN MAPS, SIMULATED (C) AND MEASURED (D) ENGINEERING MINOR STRAIN MAPS.

The deviations of the features registered at the end of the process can be reduced with an iterative compensation algorithm. The proposed algorithm suggests the compensation to be applied on the plastic tools, in order to obtain the minimization of the deviations. The compensation algorithm iteratively runs the following two main steps:

STEP I. FEM simulation: the user prepares and runs a stamping simulation, followed by a springback simulation stage and a refinement stage. During refinement, the meshes of the simulated component and the designed one are both regenerated with shell elements of approximately uniform side length. The final mesh refinement stage is very useful for performing simpler and more accurate computations at the next step II. Geometrically, the meshes are built with shell elements which represent the middle surface of the part, i.e. half of the thickness should be added in the normal direction in order to model the actual outer or inner surface of the part. As a first guess, in the first iteration of the algorithm, the deformable tools are built by offsetting the designed part by half of the initial sheet thickness.

STEP II. Compensation: the proposed algorithm has been coded within C++ and is completely automatic. The routine required the following inputs: the refined shell mesh with triangular elements of the simulated and the designed part, the outer contour of the simulated part, the external surface shell mesh of the tools in ascii. The tool geometry is modified according to the following 4 sub-steps:

II.1 Blanks mesh import and surface fitting: the meshes of simulated and designed components are imported. The nodal Cartesian coordinates of both the meshes are converted into parametric coordinates, with the library implemented in [25], as:

$$\Sigma_s = \begin{cases} x_s = x_s(u,v) \\ y_s = y_s(u,v) \\ z_s = z_s(u,v) \end{cases} \qquad \Sigma_d = \begin{cases} x_d = x_d(u,v) \\ y_d = y_d(u,v) \\ z_d = z_d(u,v) \end{cases} \qquad (2)$$

The algorithm used for the surface reconstruction is the Multilevel B-spline Approximation (MBA) [26]. Starting by the parametric coordinates, the algorithm reconstructs the surface with a recursive refinement of the B-spline knots depending on the level of desired accuracy (k). This fitting allows handling the designed and simulated objects not as numerical meshes with their nodes, but as analytical surfaces.

II.2 Tools and blank contour import: the external surface nodes of the tools and the outer contour of the simulated component are imported. The contour is useful to define the domain of the compensation.

II.3 Compensation: FIG. 13 shows a 2D graphical representation of the computed quantities. The distances δ_d and δ_s between the generic tool node $\vec{T}_0(x_{t0}, y_{t0}, z_{t0})$, and the two fitted surfaces are computed through the conjugate gradient minimization algorithm [25]. To be efficient the conjugate gradient algorithm needs a good starting point, in order to evaluate the domain of the tools node which will be involved in the compensation. Since the stamping direction of the current simulation is *z*, the *xy* plane is used as an initial guess. It is interesting to highlight that every main plane (xy, yz or xz) could be selected as initial guess, so there are no constraints related to the setup of the initial simulation. These distances are oriented in a 3D space, i.e. they are 3D vectors, with components in the Cartesian coordinates chosen for the simulation setup:

$$\vec{\delta}_s = [x_s, y_s, z_s] \qquad (3)$$

$$\vec{\delta}_d = [x_d, y_d, z_d] \qquad (4)$$

The deviation vector between the simulated and designed surfaces is defined as

$$\vec{\delta}_c = (\vec{\delta}_d - \vec{\delta}_s) \qquad (5)$$

In terms of coordinates:

$$\vec{\delta}_c = [x_{\delta c}, y_{\delta c}, z_{\delta c}] \qquad (6)$$

The tool nodes are moved from the original position $\vec{T}_0$ by the quantity $\vec{\delta}_c$. The final position of the compensated tool node is defined as:

$$\vec{T}_c = \vec{T}_0 + \lambda \vec{\delta}_c \qquad (7)$$

in terms of coordinates:

$$\vec{T}_c \begin{cases} x_{Tc} = x_{T0} + \lambda x_{\delta c} \\ y_{Tc} = y_{T0} + \lambda y_{\delta c} \\ z_{Tc} = z_{T0} + \lambda z_{\delta c} \end{cases} \qquad (8)$$

Since the final tools shape is different from the initial one, the simulation of the subsequent iterations will give back different strain distribution on the stamped component, but also different springback behavior and stresses distribution. In order to modify the compensation mechanism, the λ penalty coefficient can be tuned for controlling the strength of the compensation to be applied on the tools. As a first attempt, it is reasonable that λ=1.

Another method for influencing the quality of the compensation is by improving the quality of the tool mesh. In fact, the dimension of the $\vec{T}_c$ vector is given by the number of nodes on the tool mesh. The effectiveness of the method partly depends on the tool mesh quality, especially in the zones where larger deviations are measured.

II.4 Exporting: step 3 must be repeated for both the punch and the die**.** The meshes of both compensated tools are exported, the FEM simulation is run again and the deviations, after compensation, are calculated again.

The algorithm can be applied iteratively, as shown in Fig. 14, and the whole procedure is repeated until convergence, i.e. until the deviations between the simulated and designed parts are within the tolerance interval chosen by the designer.

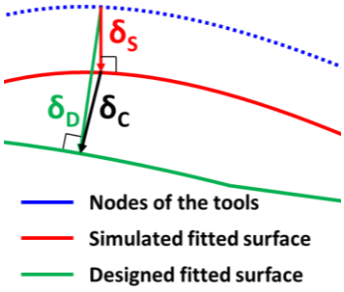

FIG. 13: COMPUTATION OF THE NEW TOOL NODES

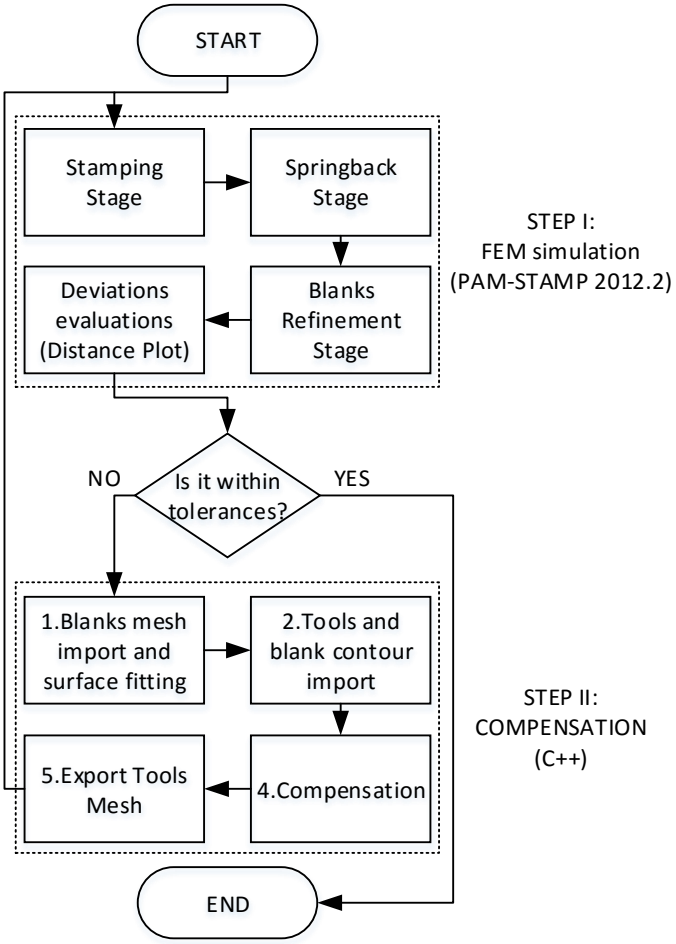

FIG. 14: FLOW CHART OF THE TOOL COMPENSATION ALGORITHM.

COMPENSATION RESULTS

In this section the results of the compensation algorithm will be presented, performed by using as an input the results of the simulation of the test case made by experiments number 3 and 10, run with BHF_{max}=22 kN.

The plot of the deviations between the simulated and designed components is shown in FIG. 15, for the whole part, including the flange. The results show that the simulated component deviates from its designed geometry in a range between [-0.59; 0.71] mm, the distribution is very scattered and only 62.3% of the calculated deviations lay within the range of [-0.22; 0.16]. This distribution of geometrical errors is unacceptable for most engineering applications. The maximum values of deviation are located on both the convex and concave corners. This corresponds to a large deformation of both tools on the corner radii (Fig. 16). Not only the deviations on the four corners are large, but the error map in Fig. 16 shows some striations, which indicate the presence of a small wrinkling phenomenon.

The algorithm performed an automatic compensation of the tools geometry, with λ=1. As a result of the first compensation, the punch and die corners radii have been modified by the algorithm in order to reduce the deviations shown in FIG. 15 and 16. After the compensation, the range of the deviations between the designed and simulated components is drastically reduced. In Fig. 17, the results of the first iteration are shown. The range of the deviations, calculated in the normal direction, lays within the range [-0.37; 0.39] mm.

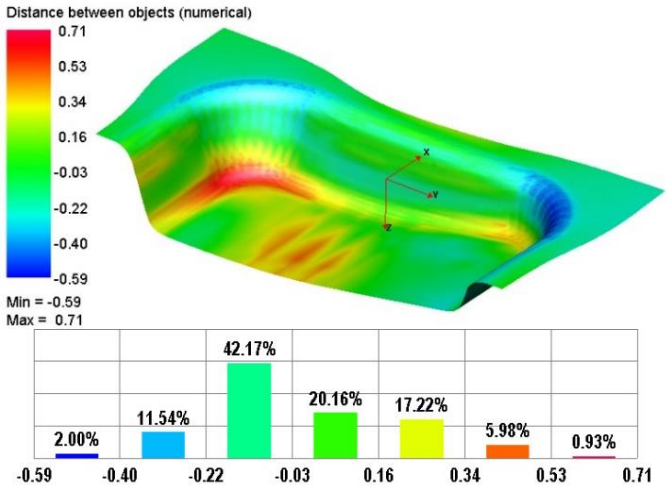

FIG. 15: δ–PLOT BEFORE COMPENSATION; ISOMETRIC AND TOP VIEWS, UNITS IN [mm].

This error range is still apparently large, but it must be noted that, unlike the view of FIG. 15 (obtained before compensation), Fig. 17 shows the larger deviations only in small regions located on the flange, i.e. out of the useful final workpiece. Furthermore, 98.3% of the surface is within the range of [-0.15; 0.18]. The range obtained already after the first compensation is therefore totally acceptable, from an engineering point of view, for many industrial applications of interest.

The evidence of wrinkling in the compensated process is practically disappeared. The maximum measured reaction force on the die increases by only 0.05 percent after compensation. The maximum measured effective stress on the tools increases by 1 MPa on the punch and by 5 MPa on the die. This means the proposed algorithm is able to reduce the geometrical errors with a negligible impact on the expected tool life.

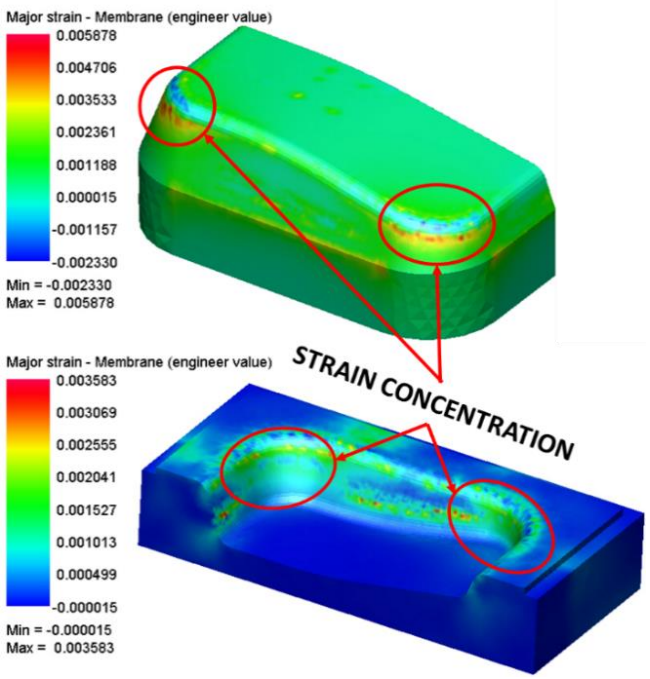

FIG. 16: STRAIN CONCENTRATIONS ON THE TOOLS AFTER THE STAMPING SIMULATION WITH NON-COMPENSATED TOOLS.

If increasing the number of iterations, the quality of the obtained solutions does not significantly improve anymore. As FIG. 18 shows, the RMS values of the deviation vector decreases drastically after the first iteration and rapidly converges towards a stable solution. Within the first 4 iterations, the best result is obtained at the second one.

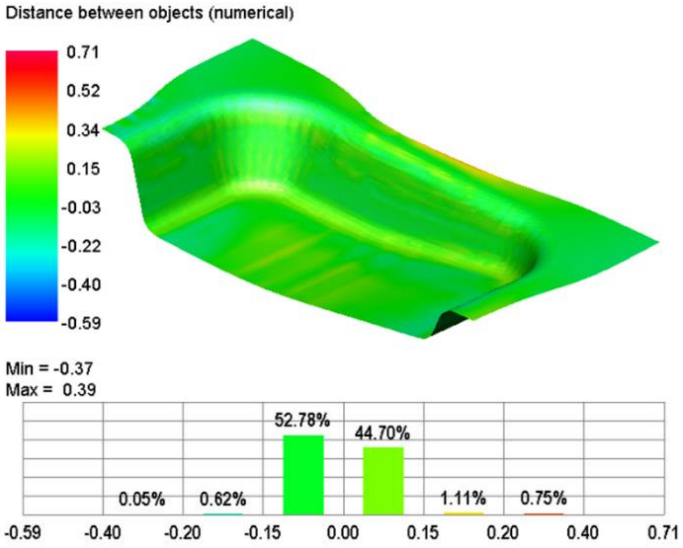

FIG. 17: DEVIATIONS BETWEEN DESIGNED AND OPTIMIZED COMPONENTS AFTER ONE ITERATION.

The calculation of the compensation $\vec{T}_c$ is performed according to equation (7) which relies on a unique value of the parameter λ, which remains constant for the whole optimization and the correct λ -value is not known a priori, it can only be guessed. In the proposed example, we have λ=1. An investigation of the role of the penalty coefficient has been conducted by comparing the RMS values of the first iterations obtained by changing the λ values from 0.8 to 1.2; the obtained results are shown in table 5. The RMS values in table 5 show that low values of penalty coefficient do not give back a complete compensation of the tools, so the RMS value is bigger. Instead, for λ-values larger than 1, the algorithm seems to improve its effectiveness. The over-compensation induced by larger penalty values not only corrects the deviations generated by the tools deformation, but also reduces the amount of the blank springback. Deepest investigations about the role of the penalty coefficient will be performed in future works: it is expected that there is an upper threshold for λ, where no further improvements can be obtained.

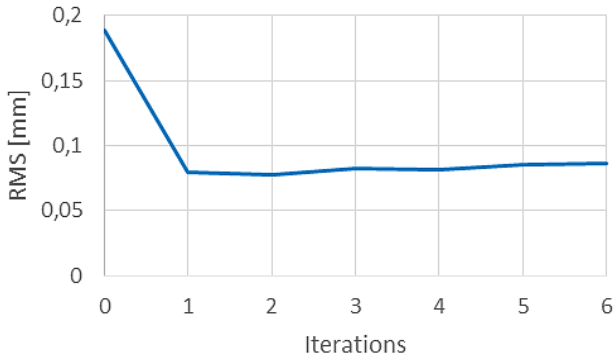

FIG. 18: NORM OF DEVIATION VECTOR VS. ITERATION.

TABLE 4: TIME NEEDED FOR 1 ITERATION.

Operation	Time needed
Simulation – 3 stages	11432 s
Reading blanks mesh	21.65 s
Parameterization	13.23 s
Compensation	90.48 s
Save tool mesh	0.07 s
Total	**11557.43 s (3.21 h)**

TABLE 5: RMS VALUES OBTAINED AFTER ONE ITERATION BY CHANGING THE λ VALUES.

λ	RMS [mm]
0.80	0.090
1.00	0.079
1.20	0.073

CONCLUSIONS

The work has demonstrated, with reference to a specific test case, that an all-polymeric (deformable) tooling setup can be used for sheet metal forming applications. The deformation of the tools can be predicted via FEM and compensated, in order to reduce within acceptable limits the deviation of the part from its nominal shape.

An FEM model for evaluating the deformations of sheet metal and polyurethane tools in a stamping process has been developed and validated.

A compensation algorithm has been proposed, based on the displacement adjustment (DA) approach. The proposed method allows to evaluate and reduce the deviations between the simulated component and the designed one. The algorithm, based on the reduction the normal deviation vector, can be applied iteratively, but in the investigated test case rapidly yields a satisfactory solution already the first iteration. The tool shape compensation does not induce a significant increase of the reaction forces and stresses on the tools.

This work represents an important step for the evolution of the deep drawing with flexible dies from a prototyping process towards a small batch, industrial manufacturing process.

ACKNOWLEDGMENTS

This project has been partly funded by the Italian National Cluster project “Fabbrica intelligente”, CTN01_00163. Mr. Corrado Buroni and Valerio Mussi of MUSP are gratefully acknowledged for their precious help in experimental tests. The authors also want to thank ViALUX for the cooperation in producing the experimental strain maps.

REFERENCES

[1] Malhotra R, Cao J, Ren F, Kiridena V, Cedric Xia ZZ, Reddy NV. Improvement of Geometric Accuracy in Incremental Forming by Using a Squeezing Toolpath Strategy with Two Forming Tools. ASME. J. Manuf. Sci. Eng. 2011;133(6):061019-061019-10. doi:10.1115/1.4005179.

[2] Del Prete A, Papadia G, Manisi B. Computer Aided Modelling of Rubber Pad Forming Process. Key Engineering Materials. 2011 Mar; 473:637–644.

[3] Son C-Y, Jeon Y-P, Kim Y-T, Kang C-G. Evaluation of the formability of a bipolar plate manufactured from aluminum alloy Al 1050 using the rubber pad forming process. Proceedings of the Institution of Mechanical Engineers, Part B: Journal of Engineering Manufacture. 2012 Jan 30;226(5):909–918.

[4] Ramezani M, Ripin ZM, Ahmad R. Sheet metal forming with the aid of flexible punch, numerical approach and experimental validation. CIRP Journal of Manufacturing Science and Technology. 2010 Jan;3(3):196–203.

[5] Giuseppe Sala. A numerical and experimental approach to optimise sheet stamping technologies: part II - aluminium alloys rubber-forming. Materials and Design. 2001; 22:299–315.

[6] Ramezani M, Ripin ZM. Analysis of deep drawing of sheet metal using the Marform process. The International Journal of Advanced Manufacturing Technology. 2011; 59(5-8):491–505.

[7] Strano M. Optimization under uncertainty of sheet-metal-forming processes by the finite element method. Proceedings of the Institution of Mechanical Engineers, Part B: Journal of Engineering Manufacture. 2006; 220(8):1305–1315.

[8] Vollertsen F, Breede R, Beckman M. Process layout and forming results from deep drawing using pressurized membranes. Proceedings of the Institution of Mechanical Engineers, Part B: Journal of Engineering Manufacture. 2001 Jan 1;215(7):977–990.

[9] Cai Z-Y, Wang S-H, Xu X-D, Li M-Z. Numerical simulation for the multi-point stretch forming process of sheet metal. Journal of Materials Processing Technology. 2009;209(1):396–407.

[10] Chua CheeKai, Leong KahFai, Liu Zhong Hong, Rapid Tooling Manufacturing, Handbook of Manufacturing Engineering and Technology, Spinger, 2014, p. 1-22.

[11] Marumo, Y., Saiki, H., & Ruan, L. (2005). Influence of resin dies and resin auxiliary sheets on deep drawability of metal foil. Journal of Materials Processing Technology, 162-163(SPEC. ISS.), 530–533.

[12] Park, Y., Colton, J.S., 2005. Failure Analysis of Rapid Prototyped Tooling in Sheet Metal Forming—V-Die Bending. J. Manuf. Sci. Eng. 127, 116.

[13] Park, Y., Colton, J.S., 2005. Failure Analysis of Rapid Prototyped Tooling in Sheet Metal Forming—Cylindrical Cup Drawing. J. Manuf. Sci. Eng. 127, 126.

[14] Park, Y., Colton, J.S., 2003. Sheet Metal Forming Using Polymer Composite Rapid Prototype Tooling. J. Eng. Mater. Technol. 125, 247.

[15] Longhi B. H., Eid C., Creative Metal forming, Brynmorgen Press, 2013.

[16] Durgun, I. (2015). Sheet metal forming using FDM rapid prototype tool, 4(January 2014), 412–422.

[17] Stratasys industrial applications: http://www.stratasys.com/solutions/additive-manufacturing/tooling/metal-hydroforming

[18] Witulski, J., Trompeter, M., Tekkaya, A. E., & Kleiner, M. (2011). High wear resistant deep drawing tools made of coated polymers. CIRP Annals - Manufacturing Technology, 60(1), 311–314.

[19] YANG, Xiang An; RUAN, Feng. A die design method for springback compensation based on displacement adjustment. International Journal of Mechanical Sciences, 2011, 53.5: 399-406.

[20] SHEN, Guozhe, et al. Springback simulation and tool surface compensation algorithm for sheet metal forming. In: AIP Conference Proceedings. IOP INSTITUTE OF PHYSICS PUBLISHING LTD, 2005. p. 334.
[21] W.H. Press, S.A. Teukolsky, W.T. Vetterling, B.P. Flannery, Numerical Recipes in C, Cambridge University Press, 1992.
[22] Karafillis A.P., Boyce M.C., Tooling and binder design for sheet metal forming processes compensation springback error. International Journal of Machine Tools & Manufacture 1996; 36 (4): 503–36.
[23] Iorio, L., Strano, M., & Monno, M. (2015). Development of a Die Compensation Algorithm for Sheet Metal Stamping with Deformable Tools. In Proceedings of the ASME MSEC International Conference, Vol. 1: Processing (p. V001T02A089). Charlotte, NC (USA).
[24] M. Amarandei, Antonio Virga, K-N. Berdich. The Influence of Defects on the Mechanical Properties of some Polyurethane Materials. Materiale Plastice, 2013; 50: 84-87.
[25] SINTEF, Geometry/GoTools, https://github.com/SINTEF-Geometry/GoTools.
[26] Lee, S., Wolberg, G., & Shin, S. Y. (1997). Scattered data interpolation with multilevel B-splines. Visualization and Computer Graphics, IEEE Transactions on, 3(3), 228-244.

Figure Captions List

Table Caption List